Available online at www.sciencedirect.com

SciVerse ScienceDirect

Procedia Computer Science 18 (2013) 1604 – 1613

Procedia Computer Science

International Conference on Computational Science, ICCS 2013

Isogeometric analysis of hyperelastic materials using PetIGA

L. M. Bernal[a], V. M. Calo[b], N. Collier[b], G. A. Espinosa[a,c], F. Fuentes[a,*], J. C. Mahecha[a]

[a]*Department of Mechanical Engineering, Universidad de los Andes, Bogotá D.C., Colombia*
[b]*Center for Numerical Porous Media (NumPor), Applied Mathematics and Computational Science, Earth and Environmental Sciences and Engineering, King Abdullah University of Science and Technology, Thuwal, Saudi Arabia*
[c]*Department of Civil Engineering, Universidad de los Andes, Bogotá D.C., Colombia*

Abstract

In this work different nonlinear hyperelastic models for slightly compressible materials are implemented in an isogeometric finite element model. This is done within the recently developed computational framework called PetIGA, which uses isogeometric analysis and modern computational tools to solve systems of equations directly and iteratively. A flexible theoretical background is described to implement other hyperelastic models and possibly transient problems in future work. Results show quadratic convergence of the nonlinear solution consistent with the Newton-Raphson method that was used. Finally, PetIGA proves to be a powerful and versatile tool to solve these types of problems efficiently.

Keywords: NURBS; isogeometric analysis; hyperelasticity; PetIGA; PETSc.

1. Introduction

Engineers often require the solution of nonlinear models that describe the physics of the problem at hand. The finite element method (FEM) has proved to be useful in solving many of these problems. Despite this, commercial software does not always provide either the versatility to model them or the computational efficiency to solve them. Hence, the need for modern computational frameworks that allow this flexibility and performance within nonlinear finite element analysis has become evident. One such framework developed recently is called PetIGA (see [1]). It uses a geometry-based Galerkin FEM, known as isogeometric analysis (IGA) (see [2]), to discretize the weak form of the partial differential equations (PDE) that govern these problems. This is valuable, taking into account the myriad of advantages that IGA offers (see [2]). Among those is the fact that, given a geometry in a specific format, there is no need for a separate discretization (meshing) procedure. The discretization of the domain along with the information required to compute the basis functions is inherent within the geometry. This is especially useful when dealing with complex geometries that may even be changing in time. Moreover, Benson et. al (in [3]) showed that IGA presents an improved performance in nonlinear problems in comparison to traditional FEM. In addition, PetIGA makes strong use of the *Portable, Extensible Toolkit for Scientific Computation* (PETSc), which is a collection of routines and data structures that essentially takes care of the linear algebra and iterative procedures in the calculations efficiently (see [4]). PETSc is applicable to large-scale simulations where computations in

*Corresponding author.
E-mail address: f.fuentes203@uniandes.edu.co.

Selection and peer review under responsibility of the organizers of the 2013 International Conference on Computational Science
doi:10.1016/j.procs.2013.05.328

parallel may be required (see [5]). In fact, PetIGA can be viewed as an extension to PETSc, and as such, has all the advantages that PETSc has.

There are many physical problems which could benefit from PetIGA to find their solution, particularly those stemming from solid mechanics. A solid under the action of a force and certain restrictions, in general, yields a nonlinear problem for the analyst. With additional assumptions, this can be ignored to obtain a linear system of differential equations, but this is not always sufficient to capture the physical behaviour. For example, when a deformed body is expected to be described by a large displacement field such as a vehicle in collision, geometrical nonlinearities cannot be neglected. In this case, by using continuum mechanics, they can be modeled and taken into account. Also, when materials can undergo large strains while still displaying purely elastic behaviour, nonlinearities may appear in the constitutive models. Examples are hyperelastic materials like rubbers and foams. It is precisely those types of materials under high displacements and strains which are considered in this article. These problems are solved using the finite element method via PetIGA under an appropriate theoretical formulation. Several constitutive models are considered. For completeness, the consistent tangent operator is presented for each of those models. The computation of this tangent considerably accelerates the convergence of the nonlinear iterative system.

2. Problem Definition

2.1. Deformation gradient, strains and stresses

A solid body in an *initial configuration* is represented by the subset $\Omega \subseteq \mathbb{R}^3$. The body then reaches a deformed state, called the *current configuration*, represented by the continuous injective mapping $\varphi : \Omega \to \mathbb{R}^3$. This way, a vector $\mathbf{X}$ representing a point of the solid in the initial configuration is mapped to the vector $\mathbf{x} := \varphi(\mathbf{X})$. Therefore, the *displacement* of the body is given by the field $\mathbf{u}(\mathbf{X}) := \mathbf{x} - \mathbf{X}$, so that $\mathbf{x} = \mathbf{X} + \mathbf{u}(\mathbf{X})$. The *deformation gradient* is defined as the tensor $\mathbf{F} := \nabla_{\mathbf{X}}\varphi(\mathbf{X}) = \nabla_{\mathbf{X}}\mathbf{x}$, which has components $\mathbf{F}_{ij} = \frac{\partial x_i}{\partial X_j}$ (in a particular basis), and determinant $J := \det(\mathbf{F})$. Using the relations above, $\mathbf{F} = \mathbf{I} + \nabla_{\mathbf{X}}\mathbf{u} = \mathbf{I} + \mathbf{H}$, where $\mathbf{H} := \nabla_{\mathbf{X}}\mathbf{u}$ is called the *displacement gradient*.

As measures of strain, the *right Cauchy-Green tensor*, $\mathbf{C} := \mathbf{F}^T\mathbf{F}$, and the *Green-Lagrange strain tensor*, $\mathbf{E} := \frac{1}{2}(\mathbf{C} - \mathbf{I})$, are defined. They operate on the initial configuration. Both are symmetric, and $\mathbf{C}$ is also positive definite. Notice that $\mathbf{E} = \frac{1}{2}(\mathbf{H} + \mathbf{H}^T + \mathbf{H}^T\mathbf{H})$, so the term $\mathbf{H}^T\mathbf{H}$ is a clear indicator of the nonlinear behavior of the Green-Lagrange strain tensor. In fact, when the components of the displacement gradient are small, it follows that $\mathbf{E} \approx \boldsymbol{\varepsilon} := \frac{1}{2}(\mathbf{H} + \mathbf{H}^T)$, where $\boldsymbol{\varepsilon}$ is the engineering (linear) strain measure. Also, $\mathbf{E}$ is invariant under rigid body motions, because when $\varphi(\mathbf{X}) = \mathbf{x} = \mathbf{Q}_\theta\mathbf{X} + \mathbf{c}$, where $\mathbf{Q}_\theta$ is a rotation (so that $\mathbf{Q}_\theta^T\mathbf{Q}_\theta = \mathbf{I}$), $\mathbf{E} = \mathbf{0}$. Both $\mathbf{E}$ and $\mathbf{C}$ are commonly used in nonlinear problems where there are large displacements (see [6, 7]).

Now, the *Cauchy stress tensor*, $\boldsymbol{\sigma}$, and the *first and second Piola-Kirchhoff stress tensors*, $\mathbf{P} := J\boldsymbol{\sigma}\mathbf{F}^{-T}$ and $\mathbf{S} := \mathbf{F}^{-1}\mathbf{P}$, are introduced, so that $\mathbf{P} = \mathbf{FS}$. The Cauchy stress tensor, which operates in the current configuration, carries its usual meaning so that by the Cauchy stress theorem, $\mathbf{t} = \boldsymbol{\sigma}\mathbf{n}$, where $\mathbf{t}$ is the traction vector and $\mathbf{n}$ is the unit normal vector to the boundary $\varphi(\partial\Omega)$ in the current configuration. The traction vector represents the force per unit area measured at a point along the boundary $\varphi(\partial\Omega)$.

As a side note, the domain of the tensor and vector fields defined above and in what follows is usually Ω. By precomposing them with φ^{-1} they can be seen as having domain $\varphi(\Omega)$. However, the precomposition implies that these are formally different fields, despite describing essentially the same behaviour. In spite of this, to lighten the notation, the corresponding fields will be referred to by the same names, and the domain will be clear from the context. Obviously, similar arguments apply if the domain of the fields was initially $\varphi(\Omega)$.

2.2. Balance of mass and linear momentum

For time-dependent problems, the solid is in a different configuration $\varphi(\Omega) = \varphi_t(\Omega)$ at each time t, where $\varphi_0(\Omega) = \Omega$. Since $\mathbf{u}$ depends on the current configuration, the *velocity* and *acceleration* are defined as $\mathbf{v} := \frac{\mathrm{d}\mathbf{u}}{\mathrm{d}t}$ and $\mathbf{a} := \frac{\mathrm{d}^2\mathbf{u}}{\mathrm{d}t^2}$ respectively. Now, the densities in the initial and current configurations are defined as ρ_0 and ρ respectively. The balance of mass in a closed system, like a solid, boils down to the equation $\rho_0 = J\rho$ (see [8] for more details). The linear momentum

$$\mathbf{L} := \int_{\varphi(\Omega)} \rho\mathbf{v}\,\mathrm{d}v = \int_{\Omega} \rho_0\mathbf{v}\,\mathrm{d}V, \tag{1}$$

which depends on the current configuration (and hence on t as well), is defined as usual, where $\mathrm{d}v$ and $\mathrm{d}V$ represent infinitesimal volume elements in the current and initial configurations respectively. The expression for the balance of mass was used in (1), where ρ_0 depends only on the initial configuration so it does not depend on time. In what follows $\mathrm{d}a$ and $\mathrm{d}A$ represent infinitesimal surface elements in the current and initial configurations respectively. The balance of linear momentum (see [6]) states that $\frac{\mathrm{d}\mathbf{L}}{\mathrm{d}t}$ is equal to the sum of all external forces (volumetric and surface) acting on the body (in the current configuration). The surface force is

$$\mathbf{R}_S := \int_{\varphi(\partial\Omega)} \mathbf{t}\,\mathrm{d}a = \int_{\varphi(\partial\Omega)} \boldsymbol{\sigma}\mathbf{n}\,\mathrm{d}a = \int_{\varphi(\Omega)} \nabla_{\mathbf{x}}\cdot\boldsymbol{\sigma}\,\mathrm{d}v = \int_{\Omega} \nabla_{\mathbf{X}}\cdot\mathbf{P}\,\mathrm{d}V, \tag{2}$$

Here, the divergence theorem along with the identity $\nabla_{\mathbf{X}}\cdot\mathbf{P} = J\nabla_{\mathbf{x}}\cdot\boldsymbol{\sigma}$ (see [8]) were used. If $\mathbf{f}$ is defined as a force field per unit mass acting on the current configuration, and $\mathbf{b} := \rho\mathbf{f}$ is the body force, the volumetric force is

$$\mathbf{R}_V := \int_{\varphi(\Omega)} \mathbf{b}\,\mathrm{d}v = \int_{\varphi(\Omega)} \rho\mathbf{f}\,\mathrm{d}v = \int_{\Omega} \rho_0\mathbf{f}\,\mathrm{d}V, \tag{3}$$

where the balance of mass was used again. Finally, the balance of linear momentum in the initial configuration asserts that

$$\int_{\Omega} \rho_0\mathbf{a}\,\mathrm{d}V = \int_{\Omega} \nabla_{\mathbf{X}}\cdot\mathbf{P}\,\mathrm{d}V + \int_{\Omega} \rho_0\mathbf{f}\,\mathrm{d}V. \tag{4}$$

This expression is also valid for any subset of Ω in the initial configuration. Hence,

$$\nabla_{\mathbf{X}}\cdot\mathbf{P} + \rho_0\mathbf{f} = \rho_0\mathbf{a}. \tag{5}$$

2.3. Hyperelastic constitutive models

A *hyperelastic material* is defined as one for which there exists a scalar function $W(\mathbf{C})$ called the *strain energy function* such that the second Piola-Kirchoff stress can be written as $\mathbf{S} = 2\frac{\partial W}{\partial \mathbf{C}}$. The function W is related to the *free Helmholtz energy function*, ψ, by $W = \rho_0\psi$. This implies that for hyperelastic materials, ψ depends exclusively on $\mathbf{C}$, so in particular, they are homogeneous. There are some properties W must satisfy for it to make physical sense (see [6, 8]), but no details will be mentioned here. Before proceeding, the fourth order tensor $\mathbb{C} := 2\frac{\partial \mathbf{S}}{\partial \mathbf{C}} = 4\frac{\partial^2 W}{\partial \mathbf{C}\partial \mathbf{C}}$ called the *material elasticity tensor* is introduced. It posseses minor symmetries (that is $\mathbb{C}_{ijkl} = \mathbb{C}_{jikl} = \mathbb{C}_{ijlk}$) as well as major symmetries (that is $\mathbb{C}_{ijkl} = \mathbb{C}_{klij}$) when derived from W.

Often materials show a different response to volumetric and deviatoric deformations. With this in mind, the strain energy function is frequently decoupled as $W(\mathbf{C}) = W_{\mathrm{iso}}(\overline{\mathbf{C}}) + W_{\mathrm{vol}}(J)$, where the *modified right Cauchy-Green tensor*, $\overline{\mathbf{C}} := J^{-2/3}\mathbf{C}$, is consistent with the split $\mathbf{F} = J^{1/3}\mathbf{I}\overline{\mathbf{F}}$ proposed in [9]. Accordingly, $\mathbf{S}$ and $\mathbb{C}$ are also split into $\mathbf{S}_{\mathrm{iso}}$, $\mathbf{S}_{\mathrm{vol}}$, $\mathbb{C}_{\mathrm{iso}}$ and $\mathbb{C}_{\mathrm{vol}}$ respectively. In view of $\det(\overline{\mathbf{F}}) = 1 = \det(\overline{\mathbf{C}})$ and $\det(J^{1/3}\mathbf{I}) = J$, it is clear that $\overline{\mathbf{F}}$, $W_{\mathrm{iso}}(\overline{\mathbf{C}})$, $\mathbf{S}_{\mathrm{iso}}$ and $\mathbb{C}_{\mathrm{iso}}$ deal with the isochoric changes, while $J^{1/3}\mathbf{I}$, $W_{\mathrm{vol}}(J)$, $\mathbf{S}_{\mathrm{vol}}$ and $\mathbb{C}_{\mathrm{vol}}$ deal with the volumetric shape-preserving changes. This approach has proved particularly useful even under high strains (finite deformations) in the context of isothermal processes [8]. The expressions for $\mathbf{S}_{\mathrm{iso}}$ and $\mathbf{S}_{\mathrm{vol}}$ are

$$\mathbf{S}_{\mathrm{iso}} = J^{-2/3}\mathbb{P} : \overline{\mathbf{S}} \quad \text{and} \quad \mathbf{S}_{\mathrm{vol}} = J\frac{\mathrm{d}W_{\mathrm{vol}}}{\mathrm{d}J}\mathbf{C}^{-1}, \tag{6}$$

where $\overline{\mathbf{S}} := 2\frac{\partial W_{\mathrm{iso}}}{\partial \overline{\mathbf{C}}}$ and the fourth order *projection tensor* is defined as $\mathbb{P} := \mathbf{I}\odot\mathbf{I} - \frac{1}{3}\mathbf{C}^{-1}\otimes\mathbf{C}$. Here, the operators $\otimes$ and : are defined as usual, so that for arbitrary $\mathbf{A}$ and $\mathbf{B}$ second order tensors and $\mathbb{A}$ and $\mathbb{B}$ fourth order tensors, $(\mathbf{A}\otimes\mathbf{B})_{ijkl} := \mathbf{A}_{ij}\mathbf{B}_{kl}$, $(\mathbf{A} : \mathbf{B}) := \mathbf{A}_{ij}\mathbf{B}_{ij}$, $(\mathbb{A} : \mathbf{B})_{ij} := \mathbb{A}_{ijkl}\mathbf{B}_{kl}$, $(\mathbf{B} : \mathbb{A})_{ij} := \mathbf{B}_{kl}\mathbb{A}_{klij}$ and $(\mathbb{A} : \mathbb{B})_{ijkl} := \mathbb{A}_{ijmn}\mathbb{B}_{mnkl}$. Additionally, the binary operator $\odot$ is defined so that $(\mathbf{A}\odot\mathbf{B})_{ijkl} := \frac{1}{2}(\mathbf{A}_{ik}\mathbf{B}_{jl} + \mathbf{A}_{il}\mathbf{B}_{jk})$, while the transpose of fourth order tensors means that $\mathbb{A}^T_{ijkl} = \mathbb{A}_{klij}$. The expressions for $\mathbb{C}_{\mathrm{iso}}$ and $\mathbb{C}_{\mathrm{vol}}$ are

$$\mathbb{C}_{\mathrm{iso}} = \tfrac{2}{3}J^{-2/3}(\overline{\mathbf{S}} : \mathbf{C})\overline{\mathbb{P}} - \tfrac{2}{3}(\mathbf{C}^{-1}\otimes\mathbf{S}_{\mathrm{iso}} + \mathbf{S}_{\mathrm{iso}}\otimes\mathbf{C}^{-1}) + J^{-4/3}\mathbb{P} : \overline{\mathbb{C}} : \mathbb{P}^T, \tag{7a}$$

$$\mathbb{C}_{\mathrm{vol}} = \Big(J\frac{\mathrm{d}W_{\mathrm{vol}}}{\mathrm{d}J} + J^2\frac{\mathrm{d}^2W_{\mathrm{vol}}}{\mathrm{d}J^2}\Big)\mathbf{C}^{-1}\otimes\mathbf{C}^{-1} - 2J\frac{\mathrm{d}W_{\mathrm{vol}}}{\mathrm{d}J}\mathbf{C}^{-1}\odot\mathbf{C}^{-1}, \tag{7b}$$

where $\overline{\mathbb{C}} := 2\frac{\partial \overline{\mathbf{S}}}{\partial \overline{\mathbf{C}}} = 4\frac{\partial^2 W_{\mathrm{iso}}}{\partial \overline{\mathbf{C}}\partial \overline{\mathbf{C}}}$ and $\overline{\mathbb{P}} := \mathbf{C}^{-1}\odot\mathbf{C}^{-1} - \frac{1}{3}\mathbf{C}^{-1}\otimes\mathbf{C}^{-1}$. Hence, by using (6) and (7), one can calculate $\mathbf{S} = \mathbf{S}_{\mathrm{iso}} + \mathbf{S}_{\mathrm{vol}}$ and $\mathbb{C} = \mathbb{C}_{\mathrm{iso}} + \mathbb{C}_{\mathrm{vol}}$.

Now, when the hyperelastic material is assumed to be *isotropic*, so that $W(\mathbf{C}) = W(\mathbf{Q}_\theta \mathbf{C} \mathbf{Q}_\theta^T)$ for any rotation tensor $\mathbf{Q}_\theta$, it follows by the representation theorem for invariants that W actually depends on the three invariants $I_1(\mathbf{C}) := \mathrm{tr}(\mathbf{C})$, $I_2(\mathbf{C})$ and $I_3(\mathbf{C}) := \det(\mathbf{C}) = J^2$ of the tensor $\mathbf{C}$ [7]. In this case, a general expression for $\mathbf{S}$ and $\mathbb{C}$ can be found in [8, (6.32), (6.193), (6.194)]. Also, when the split described above is performed, isotropy implies that W_{iso} depends solely on $\bar{I}_1 := I_1(\overline{\mathbf{C}})$ and $\bar{I}_2 := I_2(\overline{\mathbf{C}})$. In this case, general expressions for $\overline{\mathbf{S}}$ and $\overline{\mathbb{C}}$ for which only the first and second order derivatives of W_{iso} remain to be computed are

$$\overline{\mathbf{S}} = \bar{\gamma}_1 \mathbf{I} + \bar{\gamma}_2 \overline{\mathbf{C}} \quad \text{and} \quad \overline{\mathbb{C}} = \bar{\delta}_1 \mathbf{I} \otimes \mathbf{I} + \bar{\delta}_2 (\mathbf{I} \otimes \overline{\mathbf{C}} + \overline{\mathbf{C}} \otimes \mathbf{I}) + \bar{\delta}_3 \overline{\mathbf{C}} \otimes \overline{\mathbf{C}} + \bar{\delta}_4 \mathbf{I} \odot \mathbf{I}, \quad \text{where} \tag{8}$$

$$\bar{\gamma}_1 := 2\Big(\frac{\partial W_{\mathrm{iso}}}{\partial \bar{I}_1} + \bar{I}_1 \frac{\partial W_{\mathrm{iso}}}{\partial \bar{I}_2}\Big), \quad \bar{\gamma}_2 := -2\frac{\partial W_{\mathrm{iso}}}{\partial \bar{I}_2}, \quad \text{and}$$
$$\bar{\delta}_1 := 4\Big(\frac{\partial^2 W_{\mathrm{iso}}}{\partial \bar{I}_1^2} + 2\bar{I}_1 \frac{\partial^2 W_{\mathrm{iso}}}{\partial \bar{I}_1 \partial \bar{I}_2} + \frac{\partial W_{\mathrm{iso}}}{\partial \bar{I}_2} + \bar{I}_1^2 \frac{\partial^2 W_{\mathrm{iso}}}{\partial \bar{I}_2^2}\Big), \ \bar{\delta}_2 := -4\Big(\frac{\partial^2 W_{\mathrm{iso}}}{\partial \bar{I}_1 \partial \bar{I}_2} + \bar{I}_1 \frac{\partial^2 W_{\mathrm{iso}}}{\partial \bar{I}_2^2}\Big), \ \bar{\delta}_3 := 4\frac{\partial^2 W_{\mathrm{iso}}}{\partial \bar{I}_2^2}, \ \bar{\delta}_4 := -4\frac{\partial W_{\mathrm{iso}}}{\partial \bar{I}_2}. \tag{9}$$

However, it is worth mentioning that for isotropic materials, W can alternatively be formulated as depending on the eigenvalues of $\mathbf{C}$ instead of the invariants of $\mathbf{C}$, where some properties must be satisfied by this particular form of W (see [10]). With this formulation, general expressions for $\mathbf{S}$, $\mathbb{C}$, $\overline{\mathbf{S}}$ and $\overline{\mathbb{C}}$ also exist in the literature (see [8]).

2.4. Strong and weak formulations of the problem

The problem to be solved is to find the displacement field $\mathbf{u}(\mathbf{X})$ of a hyperelastic solid for every time t. The solid's initial configuration is given by Ω, while at time t its configuration is $\varphi_t(\Omega)$ and it is subjected to a fixed displacement $\mathbf{u} = \bar{\mathbf{u}}$ along $\partial_{\mathbf{u}}\Omega$ and a traction $\mathbf{t} = \bar{\mathbf{t}}$ along $\partial_\sigma\Omega$, where $\partial\Omega = \partial_{\mathbf{u}}\Omega \cup \partial_\sigma\Omega$ (so $\partial_{\mathbf{u}}\Omega \cap \partial_\sigma\Omega = \varnothing$). This boils down to finding $\mathbf{u}$ for every time t such that (5) is satisfied, when a body initially represented by Ω is subjected to the boundary conditions just mentioned, where $\varphi_t(\mathbf{X}) = \mathbf{X} + \mathbf{u}(\mathbf{X})$ and $\mathbf{P} = \mathbf{F}\mathbf{S}$ with $\mathbf{S}$ relating to $\mathbf{u}$ through $\mathbf{C}$ as described in §2.3.

The strong form of the problem stated above is difficult to solve directly. Therefore, an alternative formulation of the problem, called the weak form, is often used and is in fact the formulation on which FEM is based upon. To do this, (5) is multiplied by an appropriate vector function $\boldsymbol{\eta} \in \mathcal{V}_0$, called a *test function*, and integrated over Ω. The space $\mathcal{V}_0 := \{\boldsymbol{\eta} : \Omega \to \mathbb{R}^3 \mid \boldsymbol{\eta}(\mathbf{X}) = \mathbf{0} \text{ for } \mathbf{X} \in \partial_{\mathbf{u}}\Omega\}$ is called the *test function space*. The problem now becomes to find the displacement of the body $\mathbf{u}$ for every time t such that

$$\mathcal{N}_{\mathrm{dyn}}(\mathbf{u}, \boldsymbol{\eta}) := -\int_\Omega (\nabla_{\mathbf{X}} \cdot \mathbf{P} + \rho_0(\mathbf{f} - \mathbf{a})) \cdot \boldsymbol{\eta} \, \mathrm{d}V = \int_\Omega \mathbf{P} : \nabla_{\mathbf{X}} \boldsymbol{\eta} \, \mathrm{d}V + \int_\Omega \rho_0(\mathbf{a} - \mathbf{f}) \cdot \boldsymbol{\eta} \, \mathrm{d}V - \int_{\partial_\sigma\Omega} \mathbf{t} \cdot \boldsymbol{\eta} \, \mathrm{d}A = 0, \tag{10}$$

for every $\boldsymbol{\eta} \in \mathcal{V}_0$, when the body is subjected to the same boundary and initial conditions mentioned above. When the inertial effects can be neglected (so $\mathbf{a} \approx 0$) such as when it reaches a static equilibrium, the *static weak form* of the problem becomes that of finding $\mathbf{u}$ (notice it is a displacement which no longer depends on time) such that

$$\mathcal{N}(\mathbf{u}, \boldsymbol{\eta}) := \int_\Omega \mathbf{S} : D_{\boldsymbol{\eta}}\mathbf{E} \, \mathrm{d}V - \int_\Omega \rho_0 \mathbf{f} \cdot \boldsymbol{\eta} \, \mathrm{d}V - \int_{\partial_\sigma\Omega} \mathbf{t} \cdot \boldsymbol{\eta} \, \mathrm{d}A = 0, \tag{11}$$

for every $\boldsymbol{\eta} \in \mathcal{V}_0$, for the same boundary conditions and relations as above. In (11) it was used that

$$\mathbf{P} : \nabla_{\mathbf{X}} \boldsymbol{\eta} = \mathbf{F}\mathbf{S} : \nabla_{\mathbf{X}} \boldsymbol{\eta} = \mathbf{S} : \mathbf{F}^T \nabla_{\mathbf{X}} \boldsymbol{\eta} = \mathbf{S} : \tfrac{1}{2}(\mathbf{F}^T \nabla_{\mathbf{X}} \boldsymbol{\eta} + (\nabla_{\mathbf{X}} \boldsymbol{\eta})^T \mathbf{F}) = \mathbf{S} : D_{\boldsymbol{\eta}}\mathbf{E}, \tag{12}$$

where the symmetry of $\mathbf{S}$ was used and where the directional derivative of a tensor $\mathbf{A}(\boldsymbol{\nu})$ in the direction of the tensor $\boldsymbol{\nu}_0$ is defined as $D_{\boldsymbol{\nu}_0}\mathbf{A} := \frac{\mathrm{d}}{\mathrm{d}\varepsilon}\mathbf{A}(\boldsymbol{\nu} + \varepsilon\boldsymbol{\nu}_0)|_{\varepsilon=0}$. Here,

$$\begin{aligned} D_{\boldsymbol{\eta}}\mathbf{E} &= \tfrac{\mathrm{d}}{\mathrm{d}\varepsilon}\mathbf{E}(\varphi + \varepsilon\boldsymbol{\eta})|_{\varepsilon=0} = \tfrac{\mathrm{d}}{\mathrm{d}\varepsilon}\tfrac{1}{2}(\mathbf{F}(\varphi + \varepsilon\boldsymbol{\eta})^T \mathbf{F}(\varphi + \varepsilon\boldsymbol{\eta}) - \mathbf{I})|_{\varepsilon=0} \\ &= \tfrac{1}{2}\Big(\mathbf{F}(\varphi + \varepsilon\boldsymbol{\eta})^T \tfrac{\mathrm{d}\mathbf{F}(\varphi+\varepsilon\boldsymbol{\eta})}{\mathrm{d}\varepsilon} + \tfrac{\mathrm{d}\mathbf{F}(\varphi+\varepsilon\boldsymbol{\eta})^T}{\mathrm{d}\varepsilon}\mathbf{F}(\varphi + \varepsilon\boldsymbol{\eta})\Big)\Big|_{\varepsilon=0} = \tfrac{1}{2}(\mathbf{F}^T \nabla_{\mathbf{X}} \boldsymbol{\eta} + (\nabla_{\mathbf{X}} \boldsymbol{\eta})^T \mathbf{F}). \end{aligned} \tag{13}$$

For simplicity, from now on only the static weak form of the problem is considered.

2.5. Linearization of the weak form

In the form of the problem being considered, the functional $\mathcal{N}(\mathbf{u},\boldsymbol{\eta})$ is in general nonlinear. Many methods have been developed to try to obtain the solutions of these nonlinear problems. Among those is the *Newton-Raphson method*, which has the great advantage of displaying quadratic convergence close to the solution. Given $\mathcal{N}(\mathbf{u},\boldsymbol{\eta}) \neq 0$ for a particular $\mathbf{u}$ and some $\boldsymbol{\eta}$, the method tries to find a $\Delta\mathbf{u}$ such that $\mathcal{N}(\mathbf{u}+\Delta\mathbf{u},\boldsymbol{\eta}) = 0$ for all $\boldsymbol{\eta} \in \mathcal{V}_0$, so the final solution would easily be given by $\mathbf{u}+\Delta\mathbf{u}$. If this is not achieved, that is, if $\mathcal{N}(\mathbf{u}+\Delta\mathbf{u},\boldsymbol{\eta}) \neq 0$ for some $\boldsymbol{\eta}$, the process is repeated iteratively until convergence. The method is based on the Taylor expansion of $\mathcal{N}(\mathbf{u}+\Delta\mathbf{u},\boldsymbol{\eta})$ around $\mathbf{u}$, which is simply $\mathcal{N}(\mathbf{u}+\Delta\mathbf{u},\boldsymbol{\eta}) = \mathcal{N}(\mathbf{u},\boldsymbol{\eta}) + D_{\Delta\mathbf{u}}\mathcal{N}(\mathbf{u},\boldsymbol{\eta}) + r(\mathbf{u},\boldsymbol{\eta})$, where $r(\mathbf{u},\boldsymbol{\eta})$ represents the higher order terms. By neglecting $r(\mathbf{u},\boldsymbol{\eta})$, essentially a linearization of $\mathcal{N}$ (in its first argument) is performed. The Newton-Raphson method assumes that $0 = \mathcal{N}(\mathbf{u}+\Delta\mathbf{u},\boldsymbol{\eta}) \approx \mathcal{N}(\mathbf{u},\boldsymbol{\eta}) + D_{\Delta\mathbf{u}}\mathcal{N}(\mathbf{u},\boldsymbol{\eta})$, so that

$$D_{\Delta\mathbf{u}}\mathcal{N}(\mathbf{u},\boldsymbol{\eta}) \approx -\mathcal{N}(\mathbf{u},\boldsymbol{\eta}). \tag{14}$$

If an expression for $\Delta\mathbf{u}$ can be deduced from this relation, then the Newton-Raphson method can be used for this nonlinear problem. The term $\mathcal{N}(\mathbf{u},\boldsymbol{\eta})$ is known by use of (11). An expression for $D_{\Delta\mathbf{u}}\mathcal{N}(\mathbf{u},\boldsymbol{\eta})$ is derived next. Clearly, from (11)

$$D_{\Delta\mathbf{u}}\mathcal{N}(\mathbf{u},\boldsymbol{\eta}) = \int_\Omega D_{\Delta\mathbf{u}}(\mathbf{S} : D_{\boldsymbol{\eta}}\mathbf{E})\,\mathrm{d}V - \int_\Omega \rho_0 D_{\Delta\mathbf{u}}\mathbf{f}\cdot\boldsymbol{\eta}\,\mathrm{d}V - \int_{\partial_\sigma\Omega} D_{\Delta\mathbf{u}}\mathbf{t}\cdot\boldsymbol{\eta}\,\mathrm{d}A, \tag{15}$$

because Ω, $\partial_\sigma\Omega$ and ρ_0 are fixed and do not depend on $\mathbf{u}$, while $\boldsymbol{\eta}$ is chosen arbitrarily from $\mathcal{V}_0$ so does not depend on $\mathbf{u}$ either. For many applications, $\mathbf{f} = \mathbf{g}$, where $\mathbf{g}$ is the constant gravitational acceleration vector, and tractions $\mathbf{t}$ do not depend on the displacement field $\mathbf{u}$. Therefore, in those cases (which exclude the presence of follower forces) $D_{\Delta\mathbf{u}}\mathbf{t} = \mathbf{0} = D_{\Delta\mathbf{u}}\mathbf{f}$, and that is what will be assumed from now on. Hence, the only nonzero term left is $D_{\Delta\mathbf{u}}(\mathbf{S} : D_{\boldsymbol{\eta}}\mathbf{E}) = D_{\boldsymbol{\eta}}\mathbf{E} : D_{\Delta\mathbf{u}}\mathbf{S} + \mathbf{S} : D_{\Delta\mathbf{u}}(D_{\boldsymbol{\eta}}\mathbf{E})$. Clearly, $D_{\Delta\mathbf{u}}\mathbf{S} = \frac{\partial\mathbf{S}}{\partial\mathbf{C}} : D_{\Delta\mathbf{u}}\mathbf{C} = 2\frac{\partial\mathbf{S}}{\partial\mathbf{C}} : D_{\Delta\mathbf{u}}\mathbf{E} = \mathbb{C} : D_{\Delta\mathbf{u}}\mathbf{E}$. On the other hand, using $\mathbf{F}(\mathbf{u}) = \mathbf{I} + \nabla_{\mathbf{X}}\mathbf{u}$, (13) and that $\boldsymbol{\eta}$ does not depend on $\mathbf{u}$,

$$\begin{aligned} D_{\Delta\mathbf{u}}(D_{\boldsymbol{\eta}}\mathbf{E}) &= \tfrac{\mathrm{d}}{\mathrm{d}\varepsilon}\tfrac{1}{2}(\mathbf{F}(\mathbf{u}+\varepsilon\Delta\mathbf{u})^T\nabla_{\mathbf{X}}\boldsymbol{\eta} + (\nabla_{\mathbf{X}}\boldsymbol{\eta})^T\mathbf{F}(\mathbf{u}+\varepsilon\Delta\mathbf{u}))|_{\varepsilon=0} \\ &= \tfrac{1}{2}\Big(\tfrac{\mathrm{d}\mathbf{F}(\mathbf{u}+\varepsilon\Delta\mathbf{u})^T}{\mathrm{d}\varepsilon}\nabla_{\mathbf{X}}\boldsymbol{\eta} + (\nabla_{\mathbf{X}}\boldsymbol{\eta})^T\tfrac{\mathrm{d}\mathbf{F}(\mathbf{u}+\varepsilon\Delta\mathbf{u})}{\mathrm{d}\varepsilon}\Big)\Big|_{\varepsilon=0} = \tfrac{1}{2}\Big((\nabla_{\mathbf{X}}\Delta\mathbf{u})^T\nabla_{\mathbf{X}}\boldsymbol{\eta} + (\nabla_{\mathbf{X}}\boldsymbol{\eta})^T\nabla_{\mathbf{X}}\Delta\mathbf{u}\Big). \end{aligned} \tag{16}$$

By the symmetry of $\mathbf{S}$ it follows that $\mathbf{S} : (\nabla_{\mathbf{X}}\Delta\mathbf{u})^T\nabla_{\mathbf{X}}\boldsymbol{\eta} = \mathbf{S} : \frac{1}{2}((\nabla_{\mathbf{X}}\Delta\mathbf{u})^T\nabla_{\mathbf{X}}\boldsymbol{\eta} + (\nabla_{\mathbf{X}}\boldsymbol{\eta})^T\nabla_{\mathbf{X}}\Delta\mathbf{u}) = \mathbf{S} : D_{\Delta\mathbf{u}}(D_{\boldsymbol{\eta}}\mathbf{E})$. Finally, under the stated assumptions, (15) becomes

$$D_{\Delta\mathbf{u}}\mathcal{N}(\mathbf{u},\boldsymbol{\eta}) = \int_\Omega (\nabla_{\mathbf{X}}\boldsymbol{\eta} : \nabla_{\mathbf{X}}\Delta\mathbf{u}\mathbf{S} + D_{\boldsymbol{\eta}}\mathbf{E} : \mathbb{C} : D_{\Delta\mathbf{u}}\mathbf{E})\,\mathrm{d}V, \tag{17}$$

where, as in (13), $D_{\Delta\mathbf{u}}\mathbf{E} = \frac{1}{2}(\mathbf{F}^T\nabla_{\mathbf{X}}\Delta\mathbf{u} + (\nabla_{\mathbf{X}}\Delta\mathbf{u})^T\mathbf{F})$.

2.6. Specific constituve models

In this work, only three hyperelastic nonlinear models are considered. The first one is the St. Venant model, whose main features are described by the equations

$$W(\mathbf{C}) = \tfrac{\lambda}{2}\mathrm{tr}\Big(\tfrac{1}{2}(\mathbf{C}-\mathbf{I})\Big)^2 + \mu\mathrm{tr}\Big(\tfrac{1}{4}(\mathbf{C}-\mathbf{I})^2\Big) = \tfrac{\lambda}{2}\mathrm{tr}(\mathbf{E})^2 + \mu\mathrm{tr}(\mathbf{E}^2), \tag{18a}$$

$$\mathbf{S} = \lambda\mathrm{tr}(\mathbf{E})\mathbf{I} + 2\mu\mathbf{E}, \tag{18b}$$

$$\mathbb{C} = \lambda\mathbf{I}\otimes\mathbf{I} + 2\mu\mathbf{I}\odot\mathbf{I}, \tag{18c}$$

where λ and μ are the Lamé parameters of the given material. As mentioned in §2.1, when the elements of the displacement gradients are small, $\mathbf{S} \approx \lambda\mathrm{tr}(\boldsymbol{\varepsilon})\mathbf{I} + 2\mu\boldsymbol{\varepsilon}$, which is the usual linear stress measurement that comes accross in the literature. A similar model that satisfies the same property is the neo-Hookean model (see [6, 11]). It is described by

$$W(\mathbf{C}) = \tfrac{\mu}{2}(\mathrm{tr}(\mathbf{C}) - 3) + \tfrac{\lambda}{4}(J^2-1) - \Big(\tfrac{\lambda}{2}+\mu\Big)\ln(J), \tag{19a}$$

$$\mathbf{S} = \tfrac{\lambda}{2}(J^2-1)\mathbf{C}^{-1} + \mu(\mathbf{I}-\mathbf{C}^{-1}), \tag{19b}$$

$$\mathbb{C} = \lambda J^2\mathbf{C}^{-1}\otimes\mathbf{C}^{-1} + \Big(2\mu - \lambda(J^2-1)\Big)\mathbf{C}^{-1}\odot\mathbf{C}^{-1}. \tag{19c}$$

However, sometimes two parameters are not enough to describe a material's behavior, especially over a wide range of strains. This is usually the case with rubbers. Many models for rubbers exist to date (see [12] and [8]), but one of the first ones to be devised was that of Mooney-Rivlin [13, 14]. Its incompressible behavior is given by the equations,

$$W_{\text{iso}}(\mathbf{C}) = c_1(\bar{I}_1 - 3) + c_2(\bar{I}_2 - 3), \tag{20a}$$

$$\bar{\mathbf{S}} = 2(c_1 + c_2\bar{I}_1)\mathbf{I} - 2c_2\bar{\mathbf{C}}, \tag{20b}$$

$$\bar{\mathbb{C}} = 4c_2\mathbf{I}\otimes\mathbf{I} - 4c_1\mathbf{I}\odot\mathbf{I}. \tag{20c}$$

For the compressible part of the strain energy function W_{vol} there are a number of possibilities (see [15]), but for this work the function $W_{\text{vol}}(J) = \frac{\kappa}{\zeta^2}\Big((J^\zeta - 1) - \zeta\ln(J)\Big)$ was chosen, where κ is the bulk modulus and $\zeta > 1$ is a free parameter to be chosen.

3. Computational Model

3.1. Voigt notation

From a computational standpoint, it is useful to introduce the *Voigt notation*, where second and fourth order tensors having certain symmetries can be written as vectors and matrices respectively. In general, for a symmetric second order tensor $\mathbf{A}$ and a fourth order tensor $\mathbb{A}$ having minor symmetries, $\tilde{\mathbf{A}}$, $\check{\mathbf{A}}$, $\tilde{\mathbb{A}}$, and $\check{\mathbb{A}}$ are defined as $\tilde{\mathbf{A}} := [\mathbf{A}_{11}, \mathbf{A}_{22}, \mathbf{A}_{33}, \mathbf{A}_{12}, \mathbf{A}_{23}, \mathbf{A}_{13}]^T$, $\check{\mathbf{A}} := [\mathbf{A}_{11}, \mathbf{A}_{22}, \mathbf{A}_{33}, 2\mathbf{A}_{12}, 2\mathbf{A}_{23}, 2\mathbf{A}_{13}]^T$ and

$$\tilde{\mathbb{A}} := \begin{bmatrix} \mathbb{A}_{1111} & \mathbb{A}_{1122} & \mathbb{A}_{1133} & \mathbb{A}_{1112} & \mathbb{A}_{1123} & \mathbb{A}_{1113} \\ \mathbb{A}_{2211} & \mathbb{A}_{2222} & \mathbb{A}_{2233} & \mathbb{A}_{2212} & \mathbb{A}_{2223} & \mathbb{A}_{2213} \\ \mathbb{A}_{3311} & \mathbb{A}_{3322} & \mathbb{A}_{3333} & \mathbb{A}_{3312} & \mathbb{A}_{3323} & \mathbb{A}_{3313} \\ \mathbb{A}_{1211} & \mathbb{A}_{1222} & \mathbb{A}_{1233} & \mathbb{A}_{1212} & \mathbb{A}_{1223} & \mathbb{A}_{1213} \\ \mathbb{A}_{2311} & \mathbb{A}_{2322} & \mathbb{A}_{2333} & \mathbb{A}_{2312} & \mathbb{A}_{2323} & \mathbb{A}_{2313} \\ \mathbb{A}_{1311} & \mathbb{A}_{1322} & \mathbb{A}_{1333} & \mathbb{A}_{1312} & \mathbb{A}_{1323} & \mathbb{A}_{1313} \end{bmatrix}, \quad \check{\mathbb{A}} := \begin{bmatrix} \mathbb{A}_{1111} & \mathbb{A}_{1122} & \mathbb{A}_{1133} & 2\mathbb{A}_{1112} & 2\mathbb{A}_{1123} & 2\mathbb{A}_{1113} \\ \mathbb{A}_{2211} & \mathbb{A}_{2222} & \mathbb{A}_{2233} & 2\mathbb{A}_{2212} & 2\mathbb{A}_{2223} & 2\mathbb{A}_{2213} \\ \mathbb{A}_{3311} & \mathbb{A}_{3322} & \mathbb{A}_{3333} & 2\mathbb{A}_{3312} & 2\mathbb{A}_{3323} & 2\mathbb{A}_{3313} \\ \mathbb{A}_{1211} & \mathbb{A}_{1222} & \mathbb{A}_{1233} & 2\mathbb{A}_{1212} & 2\mathbb{A}_{1223} & 2\mathbb{A}_{1213} \\ \mathbb{A}_{2311} & \mathbb{A}_{2322} & \mathbb{A}_{2333} & 2\mathbb{A}_{2312} & 2\mathbb{A}_{2323} & 2\mathbb{A}_{2313} \\ \mathbb{A}_{1311} & \mathbb{A}_{1322} & \mathbb{A}_{1333} & 2\mathbb{A}_{1312} & 2\mathbb{A}_{1323} & 2\mathbb{A}_{1313} \end{bmatrix}. \tag{21}$$

This notation leads to many convenient expressions, which, if used appropriately, can be exploited later to give efficient computations. For example, given $\mathbf{A}_1$ and $\mathbf{A}_2$ symmetric second order tensors and $\mathbb{A}_1$ and $\mathbb{A}_2$ fourth order tensors with minor symmetries, and letting $\mathbf{A}_3 := \mathbb{A}_1 : \mathbf{A}_2$, $\mathbf{A}_4 := \mathbf{A}_1 : \mathbb{A}_2$, $\mathbb{A}_5 := \mathbb{A}_1 : \mathbb{A}_2$, $\mathbb{A}_6 := \mathbf{A}_1 \otimes \mathbf{A}_2$, and $\mathbb{A}_7 := \mathbb{A}_1^T$ leads to $\mathbf{A}_1 : \mathbf{A}_2 = \tilde{\mathbf{A}}_1 \cdot \check{\mathbf{A}}_2 = \check{\mathbf{A}}_1 \cdot \tilde{\mathbf{A}}_2 = \check{\mathbf{A}}_2^T\tilde{\mathbf{A}}_1$, $\tilde{\mathbf{A}}_3 = \tilde{\mathbb{A}}_1\check{\mathbf{A}}_2 = \check{\mathbb{A}}_1\tilde{\mathbf{A}}_2$, $\tilde{\mathbf{A}}_4 = \check{\mathbf{A}}_1\tilde{\mathbf{A}}_2$, $\tilde{\mathbf{A}}_5 = \check{\mathbb{A}}_1\tilde{\mathbf{A}}_2$, $\tilde{\mathbb{A}}_6 = \tilde{\mathbf{A}}_1\tilde{\mathbf{A}}_2^T$ and $\tilde{\mathbb{A}}_7 = \tilde{\mathbb{A}}_1^T$. Moreover, by defining $\mathbb{S} := \mathbf{I}\odot\mathbf{I}$ (because $\mathbb{S} : \mathbf{A} = \frac{1}{2}(\mathbf{A} + \mathbf{A}^T)$ for any second order tensor $\mathbf{A}$) and $\mathbb{B} := \mathbf{C}^{-1}\odot\mathbf{C}^{-1}$, (7) can be rewritten as

$$\tilde{\mathbb{C}}_{\text{iso}} = \tfrac{2}{3}J^{-2/3}(\tilde{\bar{\mathbf{S}}}\cdot\check{\mathbf{C}})\tilde{\bar{\mathbb{P}}} - \tfrac{2}{3}(\tilde{\mathbf{C}}^{-1}\tilde{\mathbf{S}}_{\text{iso}}^T + \tilde{\mathbf{S}}_{\text{iso}}(\tilde{\mathbf{C}}^{-1})^T) + J^{-4/3}\check{\mathbb{P}}\tilde{\bar{\mathbb{C}}}\check{\mathbb{P}}^T, \tag{22a}$$

$$\tilde{\mathbb{C}}_{\text{vol}} = \Big(J\tfrac{\mathrm{d}W_{\text{vol}}}{\mathrm{d}J} + J^2\tfrac{\mathrm{d}^2W_{\text{vol}}}{\mathrm{d}J^2}\Big)\tilde{\mathbf{C}}^{-1}(\tilde{\mathbf{C}}^{-1})^T - 2J\tfrac{\mathrm{d}W_{\text{vol}}}{\mathrm{d}J}\tilde{\mathbb{B}}, \tag{22b}$$

where $\tilde{\bar{\mathbb{P}}} = \tilde{\mathbb{B}} - \frac{1}{3}\tilde{\mathbf{C}}^{-1}(\tilde{\mathbf{C}}^{-1})^T$ and $\check{\mathbb{P}} = \check{\mathbb{S}} - \frac{1}{3}\tilde{\mathbf{C}}^{-1}\check{\mathbf{C}}^T$. Finally, it is worth mentioning that if a fourth order tensor $\mathbb{A}$ has minor and major symmetries, such as $\mathbb{C}$, $\mathbb{B}$, and $\mathbb{S}$ among others, then $\tilde{\mathbb{A}}$ is a symmetric matrix.

3.2. Discretization of functional space and geometry

Consider the space $\mathcal{W}_0 := \{\chi\colon \Omega \to \mathbb{R} \mid \chi(\mathbf{X}) = \mathbf{0} \text{ for } \mathbf{X} \in \partial_{\mathbf{u}}\Omega\}$ and a vector field $\mathbf{z} \in \mathcal{V}_0$. Given a certain basis of $\mathbb{R}^3$, each coordinate $z_i(\mathbf{X})$ of $\mathbf{z}(\mathbf{X}) = [z_1(\mathbf{X}), z_2(\mathbf{X}), z_3(\mathbf{X})]^T$ satisfies that $z_i \in \mathcal{W}_0$. Now, consider a finite subset $\mathcal{B} := \{N_I \in \mathcal{W}_0 \mid I = 1, \ldots, n_{\mathcal{B}}\} \subseteq \mathcal{W}_0$, which is chosen so that the linear span $\text{span}(\mathcal{B})$ is as similar to $\mathcal{W}_0$ as possible. Therefore, $\mathbf{z} \in \mathcal{V}_0$ can be approximated by $\mathbf{z}(\mathbf{X}) \approx \sum_{I=1}^{n_{\mathcal{B}}} \mathbf{z}_I N_I(\mathbf{X})$, where the $\mathbf{z}_I := [z_{1I}, z_{2I}, z_{3I}]^T \in \mathbb{R}^3$ are called the *coefficients* of $\mathbf{z}$ associated to $\mathcal{B}$ and the $N_I \in \mathcal{B}$ are called the *basis functions*. As a result, the gradient $\nabla_{\mathbf{X}}\mathbf{z}$ can also be approximated as $\nabla_{\mathbf{X}}\mathbf{z}(\mathbf{X}) \approx \sum_{I=1}^{n_{\mathcal{B}}} \mathbf{z}_I \frac{\partial N_I}{\partial \mathbf{X}}(\mathbf{X})$, where $\frac{\partial N_I}{\partial \mathbf{X}} := \left[\frac{\partial N_I}{\partial X_1}, \frac{\partial N_I}{\partial X_2}, \frac{\partial N_I}{\partial X_3}\right]$ is a row vector field. Evidently for every test function $\boldsymbol{\eta} \in \mathcal{V}_0$ these approximations are valid. Moreover, in the context of the Newton-Raphson method of the nonlinear problem being solved (see §2.5), the displacement field calculated at iteration n,

$\mathbf{u}^{(n)}$, is required to satisfy that $\mathbf{u}^{(n)} = \bar{\mathbf{u}}$ along $\partial_{\mathbf{u}}\Omega$ for every n (see §2.4). If an initial guess $\mathbf{u}^{(0)}$ is made such that this condition is satisfied, it follows that $\Delta\mathbf{u}^{(0)} = \mathbf{u}^{(1)} - \mathbf{u}^{(0)} \in \mathcal{V}_0$, and in general that $\Delta\mathbf{u}^{(n)} \in \mathcal{V}_0$. Therefore, the vector field $\Delta\mathbf{u}$ can conveniently be viewed as an element of $\mathcal{V}_0$ which also satisfies these approximations.

Now, if $D_{\mathbf{z}}\mathbf{E}_I := \frac{1}{2}\Big(\mathbf{F}^T\mathbf{z}_I\frac{\partial N_I}{\partial \mathbf{X}} + \frac{\partial N_I}{\partial \mathbf{X}}^T\mathbf{z}_I^T\mathbf{F}\Big)$, where $\mathbf{z}$ is either $\boldsymbol{\eta}$ or $\Delta\mathbf{u}$, it is clear that $D_{\mathbf{z}}\mathbf{E} \approx \sum_{I=1}^{n_{\mathcal{B}}} D_{\mathbf{z}}\mathbf{E}_I$. Furthermore, notice that $D_{\mathbf{z}}\check{\mathbf{E}}_I = \mathbf{B}_I\mathbf{z}_I$, where

$$\mathbf{B}_I := \begin{bmatrix} F_{11}\frac{\partial N_I}{\partial X_1} & F_{21}\frac{\partial N_I}{\partial X_1} & F_{31}\frac{\partial N_I}{\partial X_1} \\ F_{12}\frac{\partial N_I}{\partial X_2} & F_{22}\frac{\partial N_I}{\partial X_2} & F_{32}\frac{\partial N_I}{\partial X_2} \\ F_{13}\frac{\partial N_I}{\partial X_3} & F_{23}\frac{\partial N_I}{\partial X_3} & F_{33}\frac{\partial N_I}{\partial X_3} \\ F_{11}\frac{\partial N_I}{\partial X_2} + F_{12}\frac{\partial N_I}{\partial X_1} & F_{21}\frac{\partial N_I}{\partial X_2} + F_{22}\frac{\partial N_I}{\partial X_1} & F_{31}\frac{\partial N_I}{\partial X_2} + F_{32}\frac{\partial N_I}{\partial X_1} \\ F_{12}\frac{\partial N_I}{\partial X_3} + F_{13}\frac{\partial N_I}{\partial X_2} & F_{22}\frac{\partial N_I}{\partial X_3} + F_{23}\frac{\partial N_I}{\partial X_2} & F_{32}\frac{\partial N_I}{\partial X_3} + F_{33}\frac{\partial N_I}{\partial X_2} \\ F_{11}\frac{\partial N_I}{\partial X_3} + F_{13}\frac{\partial N_I}{\partial X_1} & F_{21}\frac{\partial N_I}{\partial X_3} + F_{23}\frac{\partial N_I}{\partial X_1} & F_{31}\frac{\partial N_I}{\partial X_3} + F_{33}\frac{\partial N_I}{\partial X_1} \end{bmatrix}. \tag{23}$$

This means $\mathbf{S} : D_{\boldsymbol{\eta}}\mathbf{E} = D_{\boldsymbol{\eta}}\check{\mathbf{E}}^T\tilde{\mathbf{S}} \approx \sum_{I=1}^{n_{\mathcal{B}}} \boldsymbol{\eta}_I^T\mathbf{B}_I^T\tilde{\mathbf{S}}$ (see §3.1). Also, $\mathbf{f}\cdot\boldsymbol{\eta} = \boldsymbol{\eta}^T\mathbf{f} \approx \sum_{I=1}^{n_{\mathcal{B}}} \boldsymbol{\eta}_I^T N_I\mathbf{f}$ and $\mathbf{t}\cdot\boldsymbol{\eta} \approx \sum_{I=1}^{n_{\mathcal{B}}} \boldsymbol{\eta}_I^T N_I\mathbf{t}$. Hence, (11) and (17) can be rewritten as

$$\mathcal{N}(\mathbf{u},\boldsymbol{\eta}) \approx \sum_{I=1}^{n_{\mathcal{B}}} \boldsymbol{\eta}_I^T\mathbf{R}_I, \quad \text{where} \quad \mathbf{R}_I := \int_\Omega \mathbf{B}_I^T\tilde{\mathbf{S}}\,\mathrm{d}V - \int_\Omega \rho_0 N_I\mathbf{f}\,\mathrm{d}V - \int_{\partial_\sigma\Omega} N_I\mathbf{t}\,\mathrm{d}A, \tag{24}$$

$$D_{\Delta\mathbf{u}}\mathcal{N}(\mathbf{u},\boldsymbol{\eta}) \approx \sum_{I=1}^{n_{\mathcal{B}}}\sum_{J=1}^{n_{\mathcal{B}}} \boldsymbol{\eta}_I^T\mathbf{K}_{IJ}\Delta\mathbf{u}_J, \quad \text{where} \quad \mathbf{K}_{IJ} := \int_\Omega (g_{IJ}\mathbf{I} + \mathbf{B}_I^T\tilde{\mathbb{C}}\mathbf{B}_J)\,\mathrm{d}V \quad \text{and} \quad g_{IJ} := \tfrac{\partial N_I}{\partial \mathbf{X}}\mathbf{S}\tfrac{\partial N_J}{\partial \mathbf{X}}^T. \tag{25}$$

In (25) it was firstly used that $D_{\boldsymbol{\eta}}\mathbf{E} : \mathbb{C} : D_{\Delta\mathbf{u}}\mathbf{E} = D_{\boldsymbol{\eta}}\check{\mathbf{E}}^T\tilde{\mathbb{C}}D_{\Delta\mathbf{u}}\check{\mathbf{E}} \approx \sum_{I,J=1}^{n_{\mathcal{B}}} \boldsymbol{\eta}_I^T\mathbf{B}_I^T\tilde{\mathbb{C}}\mathbf{B}_J\Delta\mathbf{u}_J$. The rest follows from $\nabla_{\mathbf{X}}\boldsymbol{\eta} : \nabla_{\mathbf{X}}\Delta\mathbf{u}\mathbf{S} = \mathrm{tr}(\nabla_{\mathbf{X}}\boldsymbol{\eta}^T\nabla_{\mathbf{X}}\Delta\mathbf{u}\mathbf{S})$ and $\mathrm{tr}\Big(\frac{\partial N_I}{\partial \mathbf{X}}^T\boldsymbol{\eta}_I^T\Delta\mathbf{u}_J\frac{\partial N_J}{\partial \mathbf{X}}\mathbf{S}\Big) = \boldsymbol{\eta}_I^T\Delta\mathbf{u}_J\mathrm{tr}\Big(\frac{\partial N_I}{\partial \mathbf{X}}^T\frac{\partial N_J}{\partial \mathbf{X}}\mathbf{S}\Big) = \boldsymbol{\eta}_I^T g_{IJ}\mathbf{I}\Delta\mathbf{u}_J$.

The *tangent matrix* $\mathbf{K}$, composed of all the 3×3 submatrices $\mathbf{K}_{IJ}$ can then be constructed, and similarly the *residual* $\mathbf{R} := [\mathbf{R}_1^T\cdots\mathbf{R}_{n_{\mathcal{B}}}^T]^T \in \mathbb{R}^{3n_{\mathcal{B}}}$, and the vectors $\hat{\boldsymbol{\eta}}$ and $\Delta\hat{\mathbf{u}}$ analogously. At last this leads to writing (14) in §2.5 as $\hat{\boldsymbol{\eta}}^T\mathbf{K}\Delta\hat{\mathbf{u}} \approx D_{\Delta\mathbf{u}}\mathcal{N}(\mathbf{u},\boldsymbol{\eta}) \approx -\mathcal{N}(\mathbf{u},\boldsymbol{\eta}) \approx -\hat{\boldsymbol{\eta}}^T\mathbf{R}$, so that $\mathbf{K}\Delta\hat{\mathbf{u}} \approx -\mathbf{R}$ since $\boldsymbol{\eta}$ is arbitrary. This is a linear system of equations that can then be used to implement the Newton-Raphson method described above. Only $\mathbf{K}_{IJ}$ and $\mathbf{R}_I$ have to be calculated. There are other alternative methods to solve the nonlinear problem (see [6]), but in any case, many of those methods also require the computation of the tangent matrix $\mathbf{K}$ at least once. For this, along with the computation of $\mathbf{R}$, (24) and (25) can be used.

Integration is required, in order to calculate $\mathbf{K}_{IJ}$ and $\mathbf{R}_I$. Gauss quadrature is the most common method used. However, usually a discretization of the geometry into $n_{\mathcal{E}}$ pairwise disjoint *elements* is first proposed. This way $\Omega = \cup_{e=1}^{n_{\mathcal{E}}}\Omega^e$, where Ω^e represents each element, so that one can integrate over each element independently. To take into account surface elements for the boundary conditions, the sets $\partial_\sigma\Omega^e := \partial_\sigma\Omega \cap \overline{\Omega^e}$ are defined, where the bar denotes the closure of the set. Then, in (24) the surface integral becomes $\int_{\partial_\sigma\Omega^e} N_I\mathbf{t}\,\mathrm{d}A$ elementwise, where it would be zero if $\partial_\sigma\Omega^e = \varnothing$ as usual.

This way, there would be one extra sum in (24) and (25) to approximate $\mathcal{N}(\mathbf{u},\boldsymbol{\eta})$ and $D_{\Delta\mathbf{u}}\mathcal{N}(\mathbf{u},\boldsymbol{\eta})$ respectively. However, computationally speaking this is quite inefficient. For this reason, the basis functions N_I are usually chosen so they vanish outside a certain group of elements. In fact, the discretization of Ω in elements is usually performed first, then the functional space is discretized based on the spatial discretization and finally the integration is done. In the process of the spatial discretization and the choice of the basis functions IGA offers many advantages.

Since a lot of basis functions vanish over certain elements, the sets $Z^e := \{I \mid \int_{\Omega^e} N_I\,\mathrm{d}V \neq 0\}$ are often defined for each element (a similar structure is defined computationally). Finally, (24) and (25) become

$$\mathcal{N}(\mathbf{u},\boldsymbol{\eta}) \approx \sum_{e=1}^{n_{\mathcal{E}}}\sum_{I\in Z^e} \boldsymbol{\eta}_I^T\mathbf{R}_I^e, \quad \text{where} \quad \mathbf{R}_I^e := \int_{\Omega^e} \mathbf{B}_I^T\tilde{\mathbf{S}}\,\mathrm{d}V - \int_{\Omega^e} \rho_0 N_I\mathbf{f}\,\mathrm{d}V - \int_{\partial_\sigma\Omega^e} N_I\mathbf{t}\,\mathrm{d}A, \tag{26}$$

$$D_{\Delta\mathbf{u}}\mathcal{N}(\mathbf{u},\boldsymbol{\eta}) \approx \sum_{e=1}^{n_{\mathcal{E}}}\sum_{I\in Z^e}\sum_{J\in Z^e} \boldsymbol{\eta}_I^T\mathbf{K}_{IJ}^e\Delta\mathbf{u}_J, \quad \text{where} \quad \mathbf{K}_{IJ}^e := \int_{\Omega^e} (g_{IJ}\mathbf{I} + \mathbf{B}_I^T\tilde{\mathbb{C}}\mathbf{B}_J)\,\mathrm{d}V. \tag{27}$$

3.3. PetIGA

PetIGA requires from a user the geometry, boundary conditions, and the calculation of the integrands in $\mathbf{R}_I^e$ and $\mathbf{K}_{IJ}^e$ for a general $\mathbf{X} \in \Omega^e$. For this task, PetIGA provides $\nabla_{\mathbf{X}}\mathbf{u}^{(n)}(\mathbf{X}) = \mathbf{H}^{(n)}(\mathbf{X})$, $N_I(\mathbf{X})$ and $\frac{\partial N_I}{\partial \mathbf{X}}(\mathbf{X})$, which is all that is needed in this case, where $\mathbf{u}^{(n)}$ denotes $\mathbf{u}$ in the iteration n. Then, the integration process along with the iterative solution of the problem is taken care of by PetIGA. As an option, some control over the iterative solution techniques (which are mostly already part of PETSc) is given to the user. Additionally, PetIGA allows to define arbitrary tensor product refinements of the mesh, where the user can choose the nodal spacing (h-refinement), the polynomial order (p-refinement) as well as the continuity of the basis used (k-refinement). All these are related to the accuracy of the final solution. Hence, PetIGA provides great versatility in the modeling and the process of obtaining the solution of the nonlinear problem. Moreover, this is done efficiently, because by extension of PETSc ([5]), the efficiency and ability to use parallel computing is inherited.

The geometry must be specified by *non-uniform rational basis splines* (NURBS), which are commonly used in software modeling of computer aided design geometry. Currently PetIGA requires the geometry to be globally defined with only three parametric directions which generate six surfaces. Then, a fixed value for either a Dirichlet or Neumann boundary condition (displacement or traction vector) is chosen at each surface.

4. Numerical Simulations

In order to illustrate and test the performance of the the three hyperelastic nonlinear models introduced in §2.6, numerical simulations were completed using PetIGA. The problem considered was a three dimensional hollow cylinder fixed to a wall in one end and under the uniaxial action of a tension force at the other end.

4.1. Selection of parameters of the constitutive models

Several parameters were defined for each of the hyperelastic constitutive models: St. Venant, neo-Hookean and Mooney-Rivlin (see §2.6). A rubber-like material was selected to test the behavior of all the models. The rubber bulk modulus κ, and the constants c_1 and c_2 from the Mooney-Rivlin model were taken from the literature (see [12]) and are shown in Table 1. For the St. Venant and neo-Hookean models, the Lamé parameters of the given material were calculated using $\mu = 2(c_1 + c_2)$ and $\lambda = \kappa - \frac{2}{3}\mu$ (see Table 1). Additionally, in the Mooney-Rivlin model, the parameter ζ introduced in §2.6 was taken as $\zeta = 2$.

Table 1. Material and model parameters.

Parameter	Value [MPa]
κ	1400
c_1	0.26
c_2	-0.04
μ	0.44
λ	1400

4.2. Geometry and boundary conditions

A hollow cylinder of length $L = 0.3\,\text{m}$ and internal and external radii of $R_{in} = 0.08\,\text{m}$ and $R_{out} = 0.11\,\text{m}$ was considered as the geometry for the numerical simulations. The NURBS geometry was generated using the package *Igakit* which is compatible with PetIGA (see [16]) and makes use of efficient algorithms detailed in the literature (see [17]). Three parametric directions, namely the axial, circumferential and radial directions were specified and modeled with quadratic functions. Meshes of $n_{\mathcal{D}} \times (n_{\mathcal{D}} + 3) \times n_{\mathcal{D}}$ elements were used, making reference to the axial, circumferential and radial directions respectively, and where $n_{\mathcal{D}} \in \mathbb{N}$.

Vanishing Neumann boundary conditions ($\mathbf{t} = \mathbf{0}\,\text{N/m}^2$) were chosen at all surfaces, except the two surfaces perpendicular to the axial direction, which are annuli of inner and outer radii of R_{in} and R_{out}. In one of these, zero Dirichlet boundary conditions ($\mathbf{u} = \mathbf{0}\,\text{m}$) were specified to represent the fixed end of the cylinder to the wall, while on the other Neumann boundary conditions representing a distributed axial tension force of $100\,\text{N/m}^2$ were used ($\mathbf{t} = [100, 0, 0]^T\,\text{N/m}^2$).

4.3. Results

Results were found for different values of $n_{\mathcal{D}}$ (where $n_{\mathcal{E}} := n_{\mathcal{D}}^2(n_{\mathcal{D}} + 3)$) for all three models, and the values of $|\mathbf{u}(\mathbf{X})|$ are shown in Figure 2a, where $\mathbf{X}$ is a point lying on the outer radius of the surface where the force is applied. There, it is evident that there is indeed mesh convergence and that a value of $n_{\mathcal{D}} = 14$ appears to be sufficient to obtain good accuracy of the results.

Figure 1 shows the results of the problem considered with each of the three models and $n_{\mathcal{D}} = 14$. At least the Dirichlet boundary conditions are clearly seen to be satisfied, and as expected from a physical perspective (given the tension force), the cross sections of the hollow cylinder were globally contracted in the radial direction where the force was being applied. Despite looking very similar, the results for the three models differ slightly. This can be evidenced in the change of thickness of the cylinder on the suface where the force was acting, which was initially $R_{out} - R_{in} = 0.03$m. In all three cases a decrease in thickness was observed, but the magnitude was different. Namely, for the St. Venant, neo-Hookean, and Mooney-Rivlin models the changes were of 9.8%, 9.1% and 10.3% respectively.

Regarding the method that was used to obtain the nonlinear solution, its convergence for all three models is shown in Figure 2b (again with $n_{\mathcal{D}} = 14$). There, one clearly observes the solver approaching the solution (via a line search procedure used by default in PETSc) followed by quadratic convergence of the norm of the residual towards the last iteration, which is consistent with the Newton-Raphson method and which additionally implies that the tangent matrix $\mathbf{K}$ was computed correctly. The linear solver used at each nonlinear iteration (to invert $\mathbf{K}$) was direct LU factorization. Other iterative linear solvers can be chosen within PETSc, but were not used for this work.

Additionally, the consitutive models are evidently different (see the formulas), so the computational cost to complete a simulation should vary accordingly. For comparison purposes, the computational cost was measured for the three models with the clock included in PETSc (using the same machine and processor and $n_{\mathcal{D}} = 14$). The St. Venant model took the most time (due to more iterations to converge), while the neo-Hookean and Mooney-Rivlin models took 8.88% and 9.00% less time respectively.

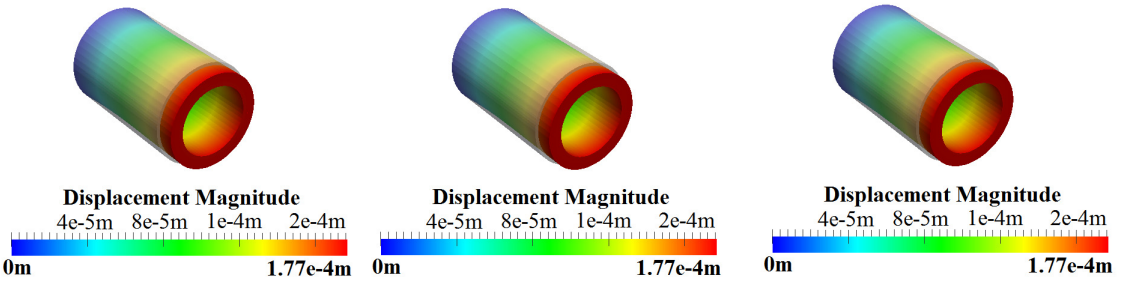

Fig. 1. Results of the numerical simulations using the St. Venant (left), neo-Hookean (middle), and Mooney-Rivlin (right) models. The initial configuration of the hollow cylinder is also shown (slightly transparent).

5. Conclusions

The three hyperelastic models proposed here in §2.6 were succesfully implemented using PetIGA. Over similar implementations, this has the feature of using isogeometric analysis, and as a result carries its advantages. Due to the fact that PetIGA is an extension of PETSc, even large-scale simulations with parallel computing can be performed efficiently. Furthermore, a flexible theoretical background was described in §2.3 to implement other nonlinear hyperelastic models quite easily using PetIGA. This could be useful for future research, since new models are being constantly developed to fit experimental data of old and new materials (see for example [18]) and researchers sometimes need an efficient high performance computational framework to test these models. With some modifications and by considering an appropriate time stepping algorithm (such as the Newmark-β

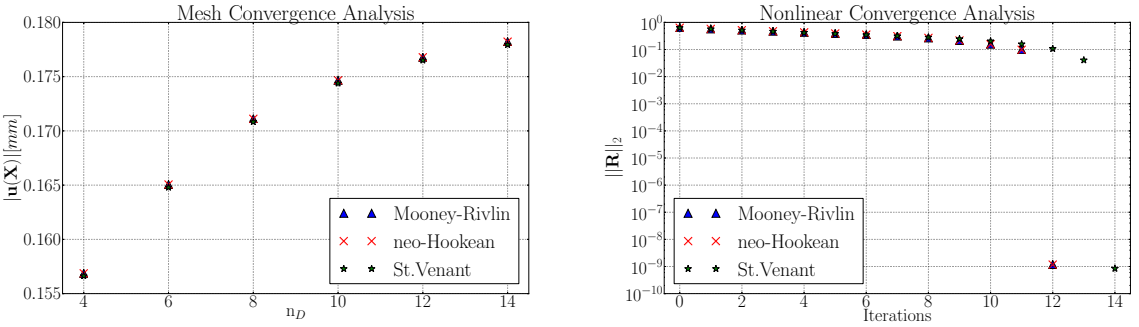

(a) Mesh convergence for all three models.

(b) Convergence of the residual Eucledian norm for all three models, with $n_{\mathcal{D}} = 14$.

Fig. 2. Convergence Analysis.

method), even transient dynamic problems can be implemented in future work. Finally, simulations of complex geometries and constitutive models better suited for biological tissues (which can be modeled as hyperelastic materials) were left for future studies.

6. Acknowledgements

The authors want to thank Universidad de los Andes and the Department of Mechanical Engineering for the 2012 summer course *Nonlinear Finite Element Analysis*, as well as the useful help provided by the reviewers.

References

[1] L. Dalcin, N. Collier, PetIGA: High performance isogeometric analysis, manuscript sumbitted for publication, package in preparation: https://bitbucket.org/dalcinl/petiga (2012).
[2] J. A. Cottrell, T. J. R. Hughes, Y. Bazilevs, Isogeometric Analysis: Toward Integration of CAD and FEA, John Wiley & Sons, New York, 2009.
[3] D. Benson, Y. Bazilevs, M. Hsu, T. Hughes, Isogeometric shell analysis: The Reissner-Mindlin shell, Computer Methods in Applied Mechanics and Engineering 199 (2010) 276 – 289.
[4] S. Balay, J. Brown, , K. Buschelman, V. Eijkhout, W. D. Gropp, D. Kaushik, M. G. Knepley, L. C. McInnes, B. F. Smith, H. Zhang, PETSc users manual, Tech. Rep. ANL-95/11 - Revision 3.3, Argonne National Laboratory (2012).
[5] S. Balay, W. D. Gropp, L. C. McInnes, B. F. Smith, Efficient management of parallelism in object oriented numerical software libraries, in: E. Arge, A. M. Bruaset, H. P. Langtangen (Eds.), Modern Software Tools in Scientific Computing, Birkhäuser Press, 1997, pp. 163–202.
[6] P. Wriggers, Nonlinear Finite Element Methods, Springer, Berlin, 2008.
[7] O. Gonzalez, A. M. Stuart, A First Course in Continuum Mechanics, Cambridege University Press, New York, 2008.
[8] G. A. Holzapfel, Nonlinear Solid Mechanics, John Wiley & Sons, West Sussex, 2000.
[9] P. J. Flory, Thermodynamic relations for high elastic materials, Trans. Faraday Soc. 57 (1961) 829–838.
[10] R. W. Ogden, Nonlinear Elastic Deformations, Cambridge University Press, New York, 1997.
[11] J. C. Simo, T. J. R. Hughes, Computational Inelasticity, Springer-Verlag, New York, 1998.
[12] P. Steinmann, M. Hossain, G. Possart, Hyperelastic models for rubber-like materials: consistent tangent operators and suitability for Treloar's data, Arch Appl Mech 82 (2012) 1183–1217.
[13] M. Mooney, A theory of large elastic deformation, Journal of Applied Physics 11 (9) (1940) 582 –592.
[14] R. S. Rivlin, Large elastic deformations of isotropic materials. IV. Further developments of the general theory, Philosophical Transactions of the Royal Society of London. Series A, Mathematical and Physical Sciences 241 (835) (1948) 379–397.
[15] S. Doll, K. Schweizerhof, On the development of volumetric strain energy functions, Journal of Applied Mechanics 67 (2000) 17–21.
[16] A. H. Niemi, N. Collier, L. Dalcin, M. Ghommem, V. M. Calo, Isogeometric shell formulation based on a classical shell model, Proceedings of the Eleventh International Conference on Computational Structures Technology.
[17] L. Piegl, W. Tiller, The NURBS Book, Monographs in Visual Communication, 1995.
[18] M. M. Carroll, A strain energy function for vulcanized rubbers, Journal of Elasticity 103 (2011) 173–187.